Journal of Inorganic and Organometallic Polymers and Materials (2020) 30:532–542
https://doi.org/10.1007/s10904-019-01213-0

Investigation of Novel Low Melting Phosphate Glasses Inside the $Na_2O–K_2O–ZnO–P_2O_5$ System

M. Jerroudi[1] · L. Bih[1,2] · M. Azrour[3] · B. Manoun[4,5] · I. Saadoune[5,6] · P. Lazor[7]

Received: 17 April 2019 / Accepted: 30 May 2019 / Published online: 4 June 2019

Abstract
Phosphate glasses containing different concentrations of zinc oxide inside the $(1-x)(NaPO_3–KPO_3)–xZnO$ system ($0 \le x \le 50$ mol%) have been prepared using the conventional melt quenching technique. The prepared glasses were transparent, bubble-free and colourless. Their density, molar volume, glass transition temperature, and structural properties using infrared and Raman spectroscopies are investigated. As the content of ZnO increases, the density increases while the molar volume decreases. The composition dependence of T_g shows a minimum for the glass ($x = 20$ mol%). Structural approach realized by IR and Raman spectroscopies reveals that zinc ions occupy different sites in the glassy-network, mainly modifier sites and middle phosphate network in low-zinc and high-zinc glasses, respectively. The introduction of ZnO in the network induces some structural rearrangements through the conversion of metaphosphate structural units to pyrophosphate ones. It is also highlighted that the presence of ZnO in the glassy matrix allows the transformation of some P–O–P and P=O bonds to P–O–Zn linkages. From the UV–Visible absorption studies, the values of the optical band gap, E_g, and Urbach energy, ΔE, were evaluated. The optical band gap is found to depend on the glasses composition. E_g and ΔE show a minimum and a maximum respectively, for the glass ($x = 20$ mol%).

Keywords Phosphate · Glasses · Glass transition temperature · Structure · Optical properties

1 Introduction

Glass is one of the most age-old materials. Since the ancient times, glass has been synthesized by the fusion of silicates. However, in recent years another glass family called phosphate glass has attracted the attention of the scientific community. These materials have been the subject of many investigations in order to use them in various applications such as the manufacturing of glass–polymer composites, glass to metal seals, optical waveguide, biomaterials, solid state laser sources, conducting materials [1–6].

Due to its hygroscopic nature, applications of P_2O_5 glass have been so limited. In order to overcome this issue, it is suggested that various oxides should be added to phosphate glasses, such as SnO, Al_2O_3, Fe_2O_3. These oxides lead to the formation of water-resist Al–O–P, Fe–O–P bonds which replace the easily hydrolysable P–O–P links and improve dramatically the chemical durability of the modified phosphate glasses [7]. Many refractory oxides can also improve the chemical durability of these phosphate glasses. However, these formulations present reticulated structures resulting in high melting temperature processing that is energy

✉ L. Bih
bihlahcen@yahoo.fr

1 Equipe de Physico-Chimie de la Matière Condensée, PCMC, Faculté des Sciences de Meknès, Meknes, Morocco

2 Département Matériaux et Procédés, ENSAM Meknès, Université Moulay Ismail, Meknes, Morocco

3 Equipe Sciences des Matériaux, Faculté des Sciences et Techniques d'Errachidia, Errachidia, Morocco

4 Laboratoire des Sciences des Matériaux, des Milieux et de la Modélisation (LS3 M), Univ Hassan 1er, 26000 Khouribga, Morocco

5 Materials Science and Nano-engineering Department, Mohammed VI Polytechnic University, Lot 660 Hay Moulay Rachid, Ben Guerir, Morocco

6 LCME, FST Marrakesh, University Cadi Ayyad, Av. A. Khattabi, BP 549, 40000 Marrakech, Morocco

7 Department of Earth Sciences, Uppsala University, Uppsala 752 36, Sweden

consuming. To develop phosphate glasses showing both good chemical durability and low temperature processing constitutes a key which has motivated many researchers to find optimal compositions. Low melting temperature and low glass transition temperature of phosphate formulations have been based for a long time on lead phosphate compositions until lead had to be replaced for toxicity reasons [8]. Promising results have been obtained using ZnO [9], SnO [10], and CuO [7]. Nevertheless, the last two oxides are subject to redox reactions during melting, so it is essential to work in a controlled atmosphere [10]. Therefore, ZnO can be considered as a best alternative for the development of stable glasses with low T_f, as evidenced by several publications [9, 11]. In addition, ZnO possesses interesting properties namely, a wide bandgap [12] and high dielectric constant values, allowing the use of ZnO in the manufacture of electronic and optical devices. It should also be noted its use in solar cells, light modulators and optical sensors [13].

The behavior of zinc in the phosphate glasses varies upon the chemical composition. This oxide alone cannot from a glass [14]. But, it can be incorporated in significant quantities in other glass forming systems such as P_2O_5 network. From the structural point of view, it is reported in the literature, that zinc oxide has a unique role since it can act both as an intermediate and as a glass modifier. Zn can exist either in ZnO_4 (tetrahedral coordination) as an intermediate component, or ZnO_6 (octahedral coordination) in the case of a network modifier [15]. The zinc phosphate system is one of many systems including $BeO–P_2O_5$ and $MgO–P_2O_5$, classified as abnormal systems since there are discontinuities in the composition/property behavior (refractive index, molar volume) [16].This abnormal behavior of the properties of the glasses was explained by a coordination change of Zn^{2+} [17, 18].

Glassy materials in the binary $(1-x)NaPO_3–xZnO$ $(0 \le x \le 33)$ were studied by Montagne et al. [19], they reported on the chemical composition dependence of some properties such as density, index of refraction, and the glass transition temperature. It is found that this latter decreases for $0 \le x \le 15$ whereas, it increases when ZnO content exceeded 15 mol% owing to the cross-linking effect of Zn^{2+} ions in the glass network. Elsewhere [12], the glasses inside $(50–x/2)\ Na_2O–xZnO–(50–x/2)P_2O_5$ system have been elaborated and it is found that the replacement of Na_2O and P_2O_5 by ZnO increased the values of the density and the glass transition temperature. The observed increase is attributed to the formation of P–O–Zn crosslinks in the glasses [11].

In this study, our interest is focused on the investigation of phosphate materials having both low melting temperature and good chemical durability. Such phosphate material could offer suitable properties in order to use them as materials for the thermal energy storage. The actual technology based on the solar salts cannot achieve a large enough difference between hot and cold storage temperature. The proposed materials contain Na_2O, K_2O, ZnO and P_2O_5 as glass former. They could present acceptable thermal and chemical stabilities and at the same time their elaboration temperature is very low. The choice of the materials is done according to the fact that: (i) the mixed alkaline effect is known to tune many physical properties and can reduce the melting temperature of the glasses; (ii) the introduction of ZnO in the glassy matrix enhances both thermal and chemical properties. The novelty of this work lies in the combination of the positive effect of ZnO to increase the chemical resistance and the mixed alkaline effect which will lead to the lowering of the melting temperature of the glasses. In particular, we are interested to study the physico-chemical and structural properties of the $(1-x)(NaPO_3–KPO_3)–xZnO$ glasses. The experimental conditions of the synthesis are determined. Their characterizations are carried out by measurements of density, thermal analysis (DSC), Infrared (IR), Raman and UV–Visible spectroscopies. Besides, we will make a comprehensive analysis on the role of zinc ions in these phosphate glasses.

2 Experimental Procedure

2.1 Preparation of the Glasses

Glasses with the compositions $(1-x)(NaPO_3–KPO_3)–xZnO$ $(0 \le x \le 50)$ were prepared by a melt-quenching route. Sodium carbonate (Na_2CO_3), potassium carbonate (K_2CO_3), hydrogen ammonium phosphate ($NH_4H_2PO_4$) and zinc nitrate ($Zn(NO_3)_2{\cdot}6H_2O$), are used as raw materials. The reagents are mixed in appropriate ratios and heated at 300 °C in order to remove NH_3 and H_2O. Then, the temperature is gradually raised to 600 °C to decompose completely the sodium and potassium carbonates. Finally, the oven temperature was increased to 1000 °C to reach the molten state. The melt was then quenched to room temperature in air by pouring it on a pre-heated plate. The obtained glass samples are colorless. They are kept in a desiccator to prevent any moisture attack.

2.2 Density Measurements and Molar Volume

Density (D) measurements of the glasses are determined at room temperature according to the Archimedes principle using distilled water ($d = 1\ g\ cm^{-3}$) as a liquid medium. The molar volume (V_m) of each glass is derived from the density and molar weight (M) values ($V_m = M/D$).

2.3 DSC Analysis

The glass transition temperature (T_g) of each glass is determined by the Differential Scanning Calorimetry (DSC). The

DSC curves were performed for ground glass batches of about 30–40 mg in a nitrogen atmosphere at a heating rate of 10 °C/min using a LABSYS evo analyzer. The estimated temperature error is ± 1 °C.

2.4 FTIR and RAMAN Spectroscopies

The infrared absorption spectra of the glasses carried out at room temperature in the wavenumber range 1400–400 cm^{-1} using a TENSOR27 spectrometer. The analysis is made on the sample pellets in KBr matrix (1:300 mg).

The structure of the studied glasses is also investigated using Raman spectroscopy in order to elucidate their structural evolution as a function of the chemical composition. Raman spectra were measured at room temperature with a Renishaw micro-Raman spectrometer (RM1000) equipped with a CCD detector, 1800 g mm^{-1} grating and an external Leica DMLM confocal microscope. The excitation source is a He–Ne laser (19 mW) operating at 632.8 nm. The laser spot was focused on the sample surface using either 50× or 100× objectives.

2.5 Optical Measurements

The optical absorption spectra of the glasses were recorded at room temperature using UV–Jasco v-750 spectrophotometer over the spectral range 200–800 nm. A barium sulfate ($BaSO_4$) plate was used as the standard (100% reflectance) on which the finely ground sample from the glass was coated.

3 Results

3.1 Physical Properties

Some physical properties of the studied glasses $(1-x)(NaPO_3–KPO_3)–xZnO$ $(0 \le x \le 50$ mol%) are gathered in Table 1. These glasses are labeled NKPZx. The composition dependence of the density, molar volume and the oxygen packing density (OPD) are given in Fig. 1. It is observed that the density and (OPD) increase while the molar volume decreases with increasing ZnO content. The thermal analysis of the glasses is carried out in order to determine their characteristic temperatures. The obtained DSC curves are shown in Fig. 2. The evolution of the glass transition temperatures (T_g) of these series of glasses as a function of the ZnO content is given in Fig. 3. It is observed that the introduction of ZnO up to 20 mol% in the network results in a decrease of T_g. For further addition of zinc oxide from 20 to 50 mol% T_g increases thereby the lowest glass transition temperature is observed for the NKPZ20 glass.

Table 1 Glass composition, O/P ratio, density, molar volume and oxygen packing density (OPD) of the $(1-x)(NaPO_3–KPO_3)–xZnO$ $(0 \le x \le 50$ mol%) glasses

Sample code	X (mol%)	O/P ratio	Density	OPD	V_m (cm^3 mol^{-1})
NKPZ0	0	3	2.44	66.52	90.19
NKPZ5	5	3.02	2.51	67.71	84.91
NKPZ10	10	3.05	2.60	69.35	79.31
NKPZ20	20	3.12	2.82	73.31	68.20
NKPZ30	30	3.21	3.03	76.40	58.89
NKPZ40	40	3.33	3.24	78.74	50.80
NKPZ50	50	3.50	3.48	80.80	43.31

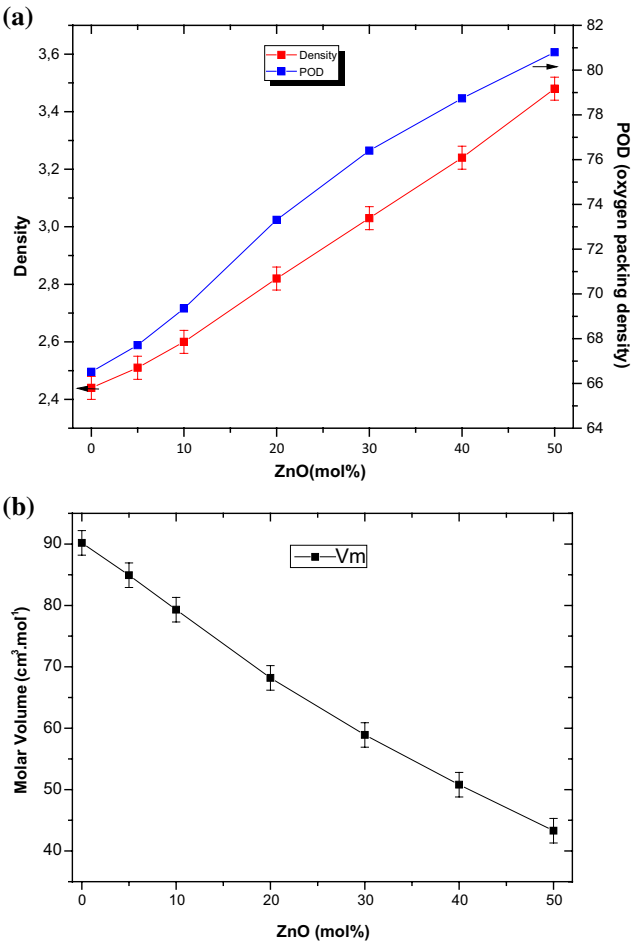

Fig. 1 The composition dependence of: **a** density, oxygen packing density, **b** molar volume

3.2 Ionocovalent Crosslink Density

From the nature of the elements constituting the glasses, one can state that the chemical bonds in the glassy-matrix could be mixture of ionic and covalent linkages. According to the ionocovalency (IC) model [20], chemical bonds depend on both their environment and the atomic properties of each element. The weight of the iconicity and covalency orders in the bond

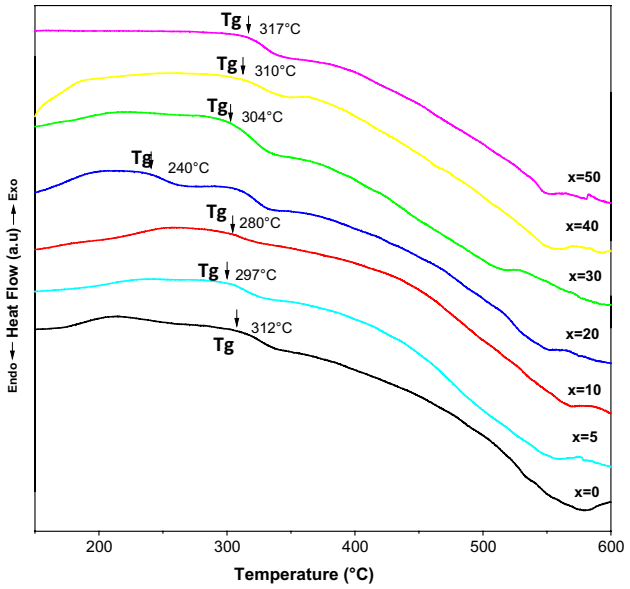

Fig. 2 DSC curves of the studied glasses

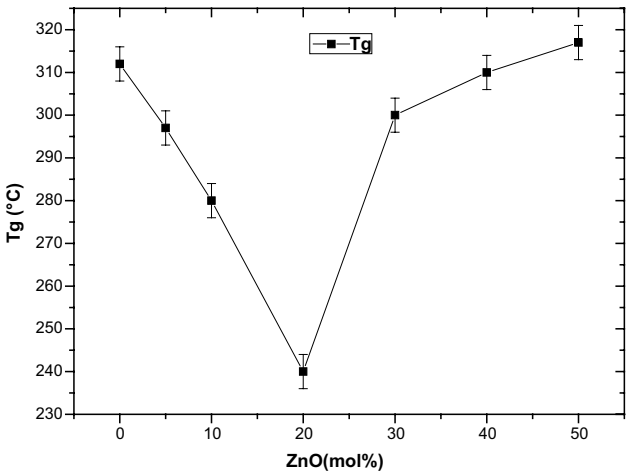

Fig. 3 The glass transition temperature (T_g) versus the composition for the glasses

defined its bond strength and effective polarizing power or charge density. The "ionocovalent crosslink density" is determined from the ionic function (I((I_a, Z*)) and the covalent function (C(($n^*r_c^{-1}$, r_c^{-1})), where n* is the effective quantum number, and r_c is the covalent radius. The ionic function, I(I_a, Z*), is related to the valency quantity of the energy required to break or re-form the ionocovalent bonds. The covalent function C ($n^*r_c^{-1}$, rc^{-1}) is related to the structural state. The covalency r_c^{-1} is related to the bond strength and the spatial covalency $n^*r_c^{-1}$ is related to the spatial overlap. The ionocovalency is defined as ionocovalent crosslink density IC_d by [21]:

$$IC_d = I(Ia,\ Z*)\ C\ (n*r_c^{-1},\ r_c^{-1}) = Z*r_c^{-1} = n*\left(I_a/R\right)^{1/2}r_c^{-1}$$

Table 2 Data of the atomic ionocovalent parameters

Glasses	x (mol%)	Z*	$n^*r_c^{-1}$	IC_d	T_g (°C)
NKPZ0	0	3.149	2.252	2.701	312
NKPZ5	5	3.164	2.277	2.712	297
NKPZ10	10	3.180	2.303	2.715	280
NKPZ20	20	3.211	2.354	2.722	300
NKPZ30	30	3.242	2.405	2.728	304
NKPZ40	40	3.274	2.456	2.734	310
NKPZ50	50	3.305	2.507	2.740	317

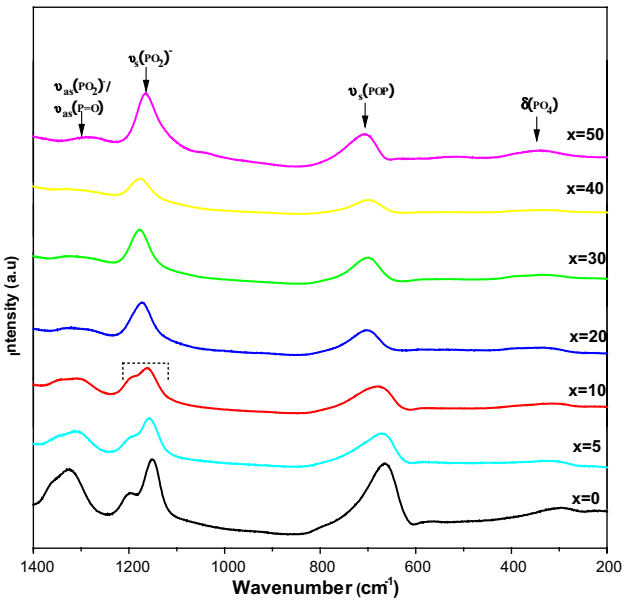

Fig. 4 Raman spectra of the $(1-x)(NaPO_3–KPO_3)–xZnO$ glasses

where I_a is the average ionization energy, Z^* is the effective nuclear charge, n^* is the effective principle quantum number, r_c is the covalent radius, R is the Rydberg constant, $R = 2\mu 42e4/h^2 = 13.6$ eV.

The application of the IC-theory to the glasses NKPZx has allowed us to determine the values of the parameters Z*, $n^*r_c^{-1}$ and IC_d and the values of these parameters are gathered in Table 2. It is noticed that the increase of the ionocovalent parameter IC_d results from the increase of both Z* and $n^*r_c^{-1}$.

3.3 Raman and IR Spectra

3.3.1 Raman Spectra

Raman spectra of $(1-x)(NaPO_3–KPO_3)–xZnO$ glasses in the 200–1400 cm^{-1} frequency range are shown in Fig. 4. This latter reveals that each spectrum contains four bands near 1324, 1153–1190, 666–710, and 340 cm^{-1}. The

assignments of the different bands are made according to the literature data [6, 11, 22, 23]. The band situated at 1324 cm^{-1} is assigned to the symmetric stretch vibration (P=O). This band can be also due to the asymmetric vibration $\nu_{as}(PO_2^-)$ of the non-bridging oxygen atoms (NBO) bonded to the phosphorus atoms (O–P–O) in metaphosphate chains (Q^2). A broad peak in the region 1153–1190 cm^{-1} is attributed to the symmetric vibration $\nu_s(PO_2^-)$ in Q^2. The band around 666–710 cm^{-1} is associated to the symmetric vibration of bridging oxygen connecting two PO_4 tetrahedra (P–O–P) in metaphosphate chains. The low frequency at 340 cm^{-1} is related to the bending motion of phosphate polyhedron. From the analysis of Fig. 5 it is observed that the intensity of the band near 1324 cm^{-1} decreases and shifts towards lower wavenumbers with increasing ZnO content. It should be noted also that the position of the peaks relatives to $\nu_s(PO_2^-)$ and ν_s(P–O–P) modes shifts to higher frequencies when ZnO content goes up (Fig. 5).

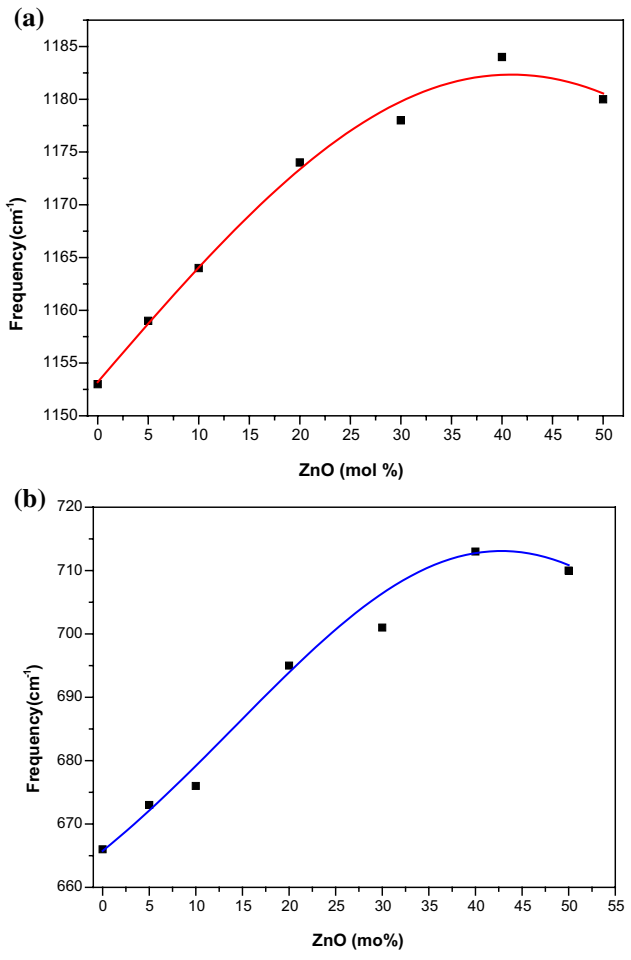

Fig. 5 Variation of the frequency position of the modes: **a** $\nu_s(PO_2)$ and **b** ν_s(P–O–P)

3.3.2 Infrared Spectra

Infrared spectra of NKPZx glasses in the range 400–1400 cm^{-1} are shown in Fig. 6. The spectra are dominated by broad bands around 1280, 1160, 1100, 1000, 900, 740, 655 and 510 cm^{-1}. Table 3 gives the positions of the different bands and their assignments. The assignment of the bands is realized taking into account the literature data [11, 23, 24]. The band near 1319–1277 cm^{-1} is related to the asymmetric stretching vibration $\nu_{as}(PO_2^-)$ in Q^2 structural unit and/or the asymmetric stretching of the doubly bonded oxygen vibration ν_{as}(P=O) in Q^3. The band at 1148–1160 cm^{-1} is ascribed to the symmetric stretching vibration $\nu_s(PO_2^-)$ in metaphosphate Q^2. The asymmetric vibration mode of the chain end group $\nu_{as}(PO_3^{2-})$

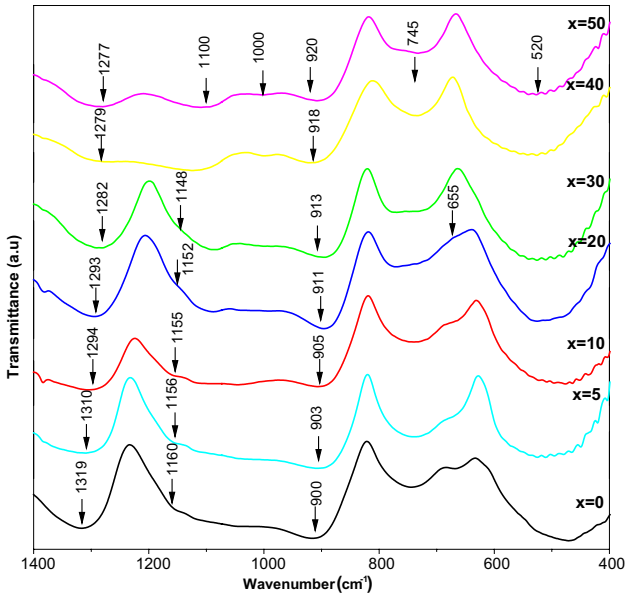

Fig. 6 Infrared spectra of the $(1-x)(NaPO_3–KPO_3)–xZnO$ glasses

Table 3 Raman and Infrared frequency positions (cm^{-1}) and their assignments

Raman frequency (cm^{-1})	Infrared frequency (cm^{-1})	Assignments
1324	1319–1277	ν_{as} (P=O), $Q^3+\nu_{as}$ (PO_2), Q^2
1153–1190	1148–1160	ν_s (PO_2), Q^2
	1100	ν_s (PO_3), Q^1
	1000	ν_s (PO_3), Q^1
	900–920	ν_{as} (P–O–P)
666–710	745	ν_s (P–O–P), Q^1
	655	ν_s (P–O–P), Q^2
340	520	$\delta(PO_4)$

corresponds to the band at 1100 cm^{-1}, and the symmetric stretching of this end group $\upsilon_s(PO_3)$ appears at 1000 cm^{-1}; the asymmetric and symmetric vibration modes of P–O–P bonds in Q^1 units, ν_{as}(P–O–P) and ν_s(P–O–P), are ascribed to bands around 920 cm^{-1} and 745 cm^{-1}, respectively. The band at about 655 cm^{-1} is attributed to the symmetric ν_s(P–O–P) in Q^2 structural groups and the band at 520 cm^{-1} is ascribed to the deformation mode of (PO_4) groups. From the analysis of the above data it can be noticed that the glass network of the glasses contains different phosphate groups and mainly metaphosphate and pyrophosphate ones.

3.3.3 Optical Spectra

The optical absorption spectra in solids provides essential information about the band structure and the energy gap in the crystalline and non-crystalline materials [25, 26]. The photons with energy greater than the band gap energy are absorbed and less energetic photons are transmitted [27]. The optical absorption spectra of the studied glasses are shown in Fig. 7. These spectra have the same shape. They are characterized by a broad onset of absorption edge over the region of 200–350 nm. Also, one can observe that the introduction of zinc oxide in the glasses doesn't induce any new absorption in the region 350–800 nm in accordance with the fact that the glasses are colorless.

From the optical absorption spectra of the glasses (Fig. 7), we have determined the energy gap and Urbach energy of the vitreous materials. The optical coefficient of absorption $\alpha(\nu)$ of each glass is calculated using the relation [25, 28]:

$$\alpha(\upsilon) = (2.303/d)A(\upsilon) \quad (1)$$

where A is the amount of absorbance and d is the thickness of the sample (in centimeter).

For amorphous materials, it is found that the optical absorption at a higher value of $\alpha(\upsilon)$ above the exponential tail follows a power law given by Davis and Mott [29]:

$$A h\upsilon = A(h\upsilon - E_g)^n \quad (2)$$

where n is an index that can have different values: 2, 3, 1/2 and 1/3 corresponding to indirect allowed, indirect forbidden, direct allowed and direct forbidden transitions, Davis and Mott proposed that most amorphous semiconductors have allowed direct transitions and (n) is 2. B is a constant called band-tailing parameter, E_g is the optical band gap energy and $h\nu$ is the incident photon energy.

In order to extract the E_g value in optical data of the glasses, it is usual to plot the variation of $(\alpha h\upsilon)^{1/2}$ as a function of $h\upsilon$ (Tauc plot). The value of the optical gap is obtained by the extrapolation of the linear region of the curve to the x-axis with $\alpha = 0$. Figure 8 represents the Tauc plots of the glasses and the obtained value of E_g are listed in Table 4. It can be seen that, the gap energy decreases with the first addition of ZnO content up to x = 20 mol%. Then, it increases with further increasing of ZnO content.

The optical data are also analyzed according to Urbach rule and the optical absorption coefficient may be written in the form [30]:

$$\alpha(\upsilon) = B \ \exp\ (h\upsilon/\Delta E) \quad (3)$$

where ΔE is the Urbach energy and B is a constant.

In view to determine the Urbach energy for the glasses we have plotted ($\ln\alpha$) versus ($h\upsilon$) as shown in Fig. 9. From the linear plot of the absorption coefficient the value of the Urbach energy ΔE can be calculated and are gathered in Table 4. It is observed that the Urbach energy (ΔE) increases

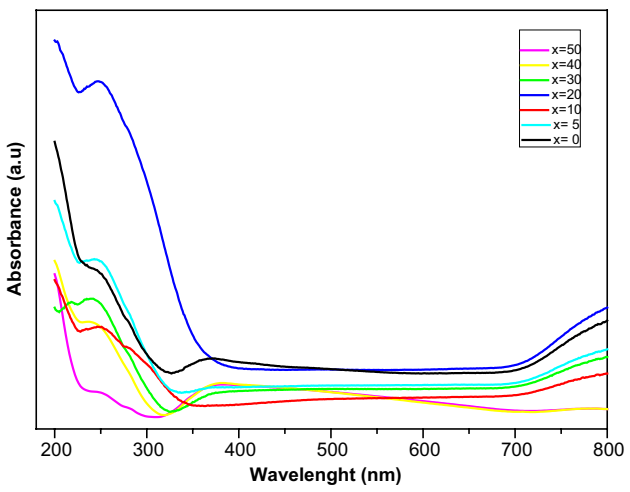

Fig. 7 Optical absorption spectra in the range 200–800 nm for the studied glasses

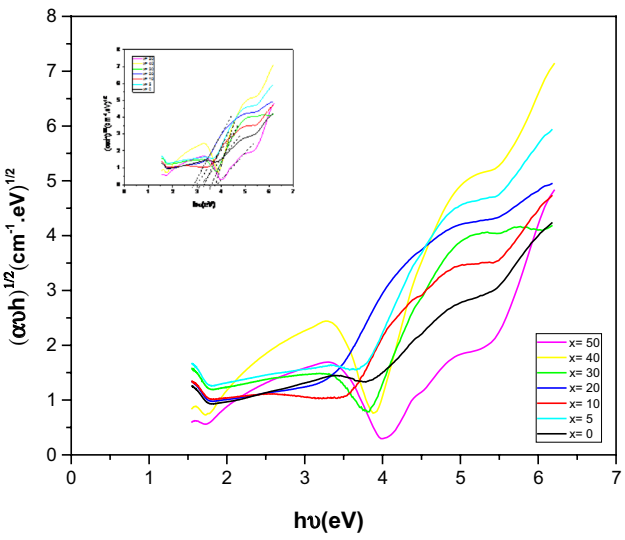

Fig. 8 Variation of $(\alpha h\upsilon)^{1/2}$ as a function of photon energy ($h\upsilon$) for the studied glasses

Table 4 Optical band gap and Urbach energy of the $(1-x)$ $(NaPO_3–KPO_3)$–xZnO glasses

x (mol%)	Optical band gap E_{opt} (eV)	Urbach energy ΔE (eV)
0	3.35	0.227
5	3.30	0.253
10	3.01	0.260
20	2.88	0.277
30	3.60	0.239
40	3.79	0.237
50	3.84	0.181

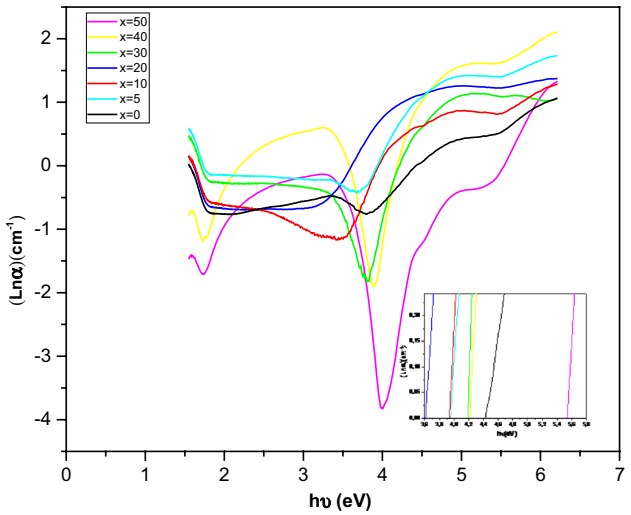

Fig. 9 Variation of ln(α) as a function of photon energy (hυ) for the glasses

with increasing ZnO content when the concentration of ZnO varies from x = 0 to x = 20 mol%, then it decreases with further addition of ZnO content (x > 20 mol%) (Fig. 10).

4 Discussion

4.1 ZnO Effect on the Physical Properties of the Glasses

The variation of the density as a function of ZnO content (Fig. 1) shows an increase of the density from 2.44 to 3.48 with increasing ZnO content which suggests that the incorporation of zinc oxide in the glass network induces an increase in the compactness of the glassy structure. In order to confirm such ZnO effect on the density, we have calculated the oxygen packing density (OPD) of the glasses (Fig. 1). It is found that the OPD parameter increases with the increase of ZnO content suggesting an increase in the

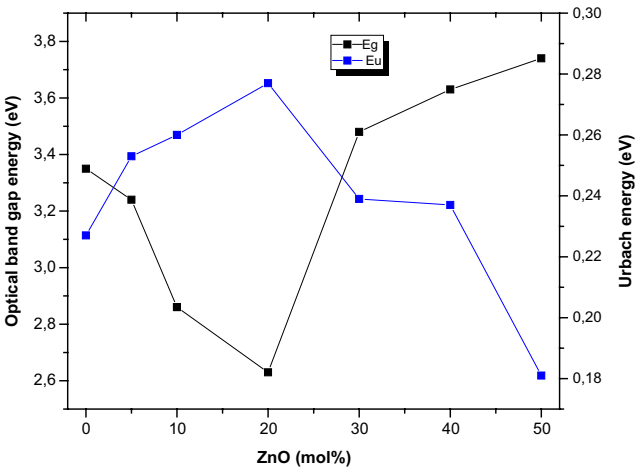

Fig. 10 The composition dependence of the optical gap and Urbach energy

connectivity of the polyhedral and thereby an increase in the density of links in the glass network.

Moreover, the density parameter is a physical property which is sensitive to the spatial arrangements of atoms in the vitreous network. It depends on several factors namely, the structure, the molecular weight, the coordination number, and the dimensionality of the interstitial space. According to these parameters, the observed increase of the density with ZnO content in the $(1-x)$ $(NaPO_3–KPO_3)$–xZnO glasses could be associated to the replacement of the ionic linkages (PO^-, Na^+) and/or (PO^-, K^{+}) issued from the matrix $(NaPO_3–KPO_3)$ by the ionocovalent P–O–Zn bonds. The presence of these latters bond-type enhances the connectivity, the reticulation and renders the glassy structure denser at high ZnO content. A similar evolution of density was obtained in the $(1-x)NaPO_3$–xZnO glasses [19]. From Fig. 1, it is observed that the molar volume decreases when the ratio of ZnO increases. This decrease could be associated with the decrease of the interstitial space between the polyhedra which is induced by the reticulation effect of zinc ions. It seems that the increase of connectivity between polyhedra reduces the inter-atomic distances so that the molar volume decreases and the density increases. Furthermore, the increase in density as a function of the composition (x) cannot be interpreted in terms of the increase of molecular weight since the molar weight of $NaPO_3–KPO_3$ ($M = 220.07$ g mol^{-1}) is higher than that of ZnO ($M = 81.38$ g mol^{-1}).

The glass transition temperature is also sensitive to the structure of the glasses [26, 31]. It depends on bond strength, degree of crosslink density and packing tightness. The glass transition temperature is an increasing function of these variables [31]. The variation of the glass transition temperature as a function of ZnO content in the glassy network is

shown in Fig. 3. It shows a minimum when ZnO addition reaches 20 mol%. Thus, the composition dependence of T_g can be divided to low-ZnO and high-ZnO regions in which Zn^{2+} ions occupied different sites. The observed decrease of T_g in the low-ZnO region reveals that the introduction of zinc oxide in the network do not enhance the crosslink density of the phosphate network. It seems that the sites occupied by Zn^{2+} ions in this low-ZnO region are positions mainly located near the end phosphate chains, mainly near the pyrophosphate groups (Q^1, sites). The Zn^{2+} ions in these end sites are not able to enhance the crosslink density of the glassy-matrix. On the other hand, for the high-ZnO region, $x > 20$ mol%, the glass transition temperature increases. The increase of the bond strength and the tightness of the network in this region are involved in the observed increase of T_g. The increase of the bond strength is due to the fact that the glasses are poor in Na_2O and K_2O and become more covalent by the formation of P–O–Zn bonds in vitreous network of the glasses belonging to the high-ZnO region. Moreover, the observed T_g in this region indicates that the Zn^{2+} ions can also enhance the crosslink in the glass network owing to the reticulation effect. It seems that these zinc ions are located in sites allowing the increase of the crosslink density. One can suppose that these sites are located between phosphate chains rather than end chains. Therefore, one can conclude that the structural sites occupied by Zn^{2+} ions in low-ZnO and high-ZnO regions are different. The occupation of the end sites decreases T_g whereas the presence of zinc in the middle of phosphate chains reticulates the network and thereby increases the glass transition temperature. The observed minimum of T_g at $x = 20$ mol% can be due to the combination of the two above effects. Moreover, it is reported that mixed alkali and mixed alkaline–alkaline earth in glasses induce the presence of minima in the composition variation of some properties such as T_g [32–34]. In $(1-x)(NaPO_3–KPO_3)–xZnO$ glasses, the ratio Na/(Na+K) is constant and has a fixed value of 0.5. This means that the mixed alkali effect is not responsible for the observed minimum for T_g. Therefore, this minimum of T_g at $x = 20$ mol% could be ascribed also to the substitution of alkaline ions (Na^+, K^+) by a divalent Zn^{2+} cations.

Let us now discuss the effect of the crosslink density IC_d as a function of the composition. This parameter depends on two functions (I, C): the ionic dynamics represented by the function $I(I_a, Z^*)$, and the covalent structures by C (rc^{-1}, n^*rc^{-1}). The determined ionocovalent parameters are given in Table 2. It is observed that Z* as iconicity parameter increases when the ratio of zinc goes up. Z* is related to the valency quantity of the energy required to break the P–O–P bonds and re-form the crosslink density [20]. On the other hand, the n^*rc^{-1} parameter describes the amount of mixing of oxygen 2*p* and metal orbitals to form valence bands. The variation of n^*rc^{-1} as a function of the composition (Table 2) shows an increase with ZnO content suggesting that zinc 3d and oxygen 2p orbitals are overlapped. Therefore, the increase of the crosslink density with zinc oxide can be attributed to the increase of both Z* and n^*rc^{-1} in agreement with the IC-model $IC_d = I(I_a)C(n^*r_c^{-1}) = n^*(I_d/R)^{1/2}r_c^{-1}$. The Zn 3*d* orbitals, compared to P *3p* orbitals, involved the greater spatial covalency, $n^*r_c^{-1}$, leading to a greater overlap with oxygen *2p* orbitals. The ionic and the covalent functions are combined to give a quantification result of ionocovalent crosslink density IC_d from 2.701 to 2.740 (Table 2). The increase of this parameter with increasing zinc content explains well the increase of the density and the decrease of the molar volume (Table 1). It can also argue the increase of the glass transition temperature T_g from 240 to 317 °C in the composition range from 20 to 50 mol% of zinc oxide.

4.2 ZnO Effect on the Structure of the Glasses

4.2.1 Raman Spectra

The introduction of ZnO into the $(NaPO_3–KPO_3)$ network brings some modifications on the Raman spectra (Fig. 4). A displacement towards the high wavenumbers of the mode relative to $\nu_s\,(PO_2)^-$ is observed between 1153 and 1180 cm^{-1}. Also, we observe that the position of the vibration mode of ν_s(P–O–P) is shifted to high frequency (Fig. 5). Firstly, these two modifications can be explained by the fact that the electronegativity of Zn (1.65) is higher than that of Na(0.93) and K(0.82) [35]. In fact, the increase in electronegativity around the phosphate groups $(PO_2)^-$ and (P–O–P) induces the shift of these frequencies towards the high frequencies [36]. Secondly, the substitution of the larger Na^+ (95 pm) and K^+ (133 pm) cations by smaller size Zn^{2+} ions (74 pm) [37], can cause the decrease of the (OPO) angle resulting in a steady increase of the vibration energy of (P–O–P) and then the displacement of this mode to high wavenumbers. Moreover, the shape of the peak associated with $\nu_s(PO_2)^-$ in the region 1153–1190 cm^{-1} changes with ZnO content in the network. In the Raman spectrum of the ZnO-free glass ($x = 0$), this peak is composed by two components which are due to the presence of two PO_2^- groups linked to different cations (Na^+ and K^+). Particularly, the vibration of P–O in (PO_2^-, K^+) unit is reinforced in comparison with that of P–O in (PO_2^-, Na^+) component. So, the vibration mode of (PO_2^-, K^+) is ascribed to the component at high wavenumbers (1193 cm^{-1}) whereas, the frequency of (PO_2^-, Na^+) appears at low wavenumbers (1153 cm^{-1}). From the spectra of Fig. 4, we observe that the two components of $\nu_s(PO_2)^-$ emerge to form only one broad peak at high wavenumbers for the glasses belonging to the high-ZnO region (20–50 mol%). However, for the glasses of the low-ZnO region (0–20 mol%) the intensity of the two components decreases suggesting that Zn^{2+} replaces Na^+ and K^+ cations.

Therefore, in this low ZnO-region one can state that Zn^{2+} ions occupy the modifier sites previously occupied by the alkali elements. In the high-ZnO region, it seems that zinc ions occupy new sites that allows the increase of the crosslink density of the glasses. Moreover, the Raman spectra reveal the disappearance of the P=O mode at 1324 cm^{-1} as the concentration of ZnO increases in the vitreous network. This, can be explained by the conversion of P=O bonds into P–O–Zn linkages.

4.2.2 FTIR Spectra

From the analysis of IR spectra of the studied glasses (Fig. 6), it is observed that the addition of ZnO in the glassy matrix influences the intensity and the position of some bands. The asymmetric vibration mode of $(PO_2)^-$ shifts to lower wavenumbers as the content of ZnO increases. This decrease is associated with the higher field strength of Zn^{2+} in comparison to that of alkali Na^+ and K^+ ions. In fact, when the metal–oxygen force constant increases it is expected that the vibration energy of the neighborhood PO_2 group decreases [38, 39]. Figure 6, also shows changes in the position and the intensity of the vibration modes $\nu_s(PO_2)^-$ and $\nu_s(PO_3)^{2-}$. When the concentration of zinc oxide increases it is observed that the position of the mode $\nu_s(PO_2)^-$, near 1160 cm^{-1}, shifts to lower wavenumbers owing to higher strength of Zn–O bonds. The intensity increase of the peak at about 1100 cm^{-1}, characteristic of $\nu_s(PO_3)^{2-}$, suggests that more pyrophosphate units are created in the network with increasing zinc oxide content. As a matter of fact, the introduction of ZnO in the glasses is accompanied by the increase of the O/P ratio (Table 1) from 3 to 3.5 suggesting that the substitution of ($NaPO_3$–KPO_3) by ZnO induces the formation of pyrophosphate Q^1 units in the detriment of metaphosphate Q^2 units. The formation of pyrophosphate units is also confirmed since the intensity of the band at 745 cm^{-1} increases in the zinc-rich glasses (Fig. 6). It seems that the environment of zinc ion in these glasses becomes richer in pyrophosphate units. The formation of strong P–O–Zn bonds in their networks is very likely since the position of the mode ν_{as}(P–O–P) shifts from 900 to 920 cm^{-1} with zinc content in the glasses. Therefore, one can state that some P=O and P–O–P bonds are converted to P–O–Zn links when ZnO content increases in the vitreous network.

4.2.3 Optical Spectra

The analysis of the optical absorption spectra (Fig. 7) reveals the presence of a broad band around 200–350 nm which is characteristic of amorphous materials [40]. The presence of this ultraviolet absorption band may be due to two main causes: (i) The electron transition between oxygen 2p and transition metal 3d, (ii) the presence of impurity ions such as Fe^{3+} [40].

The composition dependence of the gap energy (Table 4) shows that E_g decreases in the composition range from 0 to 20 mol% ZnO (low ZnO region). In a previous study [40], it is observed that the gap energy E_g decreased with increasing alkali ions in phosphate, silicate and borate glasses. The tendency has been explained by the increase of the non-bridging oxygen (NBO) ions in the glasses. As a matter of fact, the introduction of modifier oxide in the glassy-matrix modifies the network and creates non-bridging oxygen atoms. Therefore, the observed decrease of the E_g energy in the range 0–20 mol% of ZnO suggests that zinc ion has a modifier structural effect in agreement with IR and Raman studies. Moreover, it seems that the substitution of alkali ions by zinc ones in the low-ZnO region glasses is realized in the way that Zn^{2+} ions locate in the modifier sites which were already occupied by the alkali ions (Na^+ and K^+). In other words, in the low-ZnO glasses, (0–20 mol%), Zn^{2+} ion plays the modifier structural role as alkali ions. So, the variation of E_g in the lower-ZnO region may be interpreted on the basis that the effect of ZnO is to increase the non-bridging oxygen in the glasses. It is known that the (BO) atom has lower energy, and has also a less negative charge than (NBO). The existence of more NBO in the glass affects the gap energy so that the electrons transfer easily from the valence band to the conduction band in rich-NBO glasses [25]. It is worth to note that the optical energy gap depends on the energy level of the upper valence band edge, which is determined by the separation of 3d states and 2p oxygen states [40]. In the low-ZnO glasses, it seems that the substitution of alkali ions (Na^+ and K^+) by zinc ions (Zn^{2+}) induces two concomitant effects: firstly, the formation of NBO ions and causes an increase in 2p oxygen energy levels; secondly an increase of the covalent character of the bonds since the electronegativity of zinc is higher than that of alkali ions, this increase of bond strength causes a decrease of the optical energy gap [40]. All these facts act in the same trend and resulting in a smaller band gap in the lower-ZnO region. However, in the high-ZnO glasses with $x > 20$ mol% the gap energy increases when the content of zinc oxide goes up (Table 4). This increase suggests that in high-ZnO region the Zn^{2+} ions are located in sites that allows reducing the concentration of non-bridging oxygen atoms in the network of the glasses. These novel sites for Zn^{2+} ions are able to enhance the crosslink density of the glassy matrix as emphasized by the ionocovalency (IC_d) studies. Therefore, one can assume that Zn^{2+} ions introduce the glassy-matrix and locate between phosphate chains rather than end chains. The occupation of these kinds of sites induces the decrease in the NBO number and thereby the increase of E_g for the high-ZnO glasses.

Moreover, the analysis of the optical data has revealed that the variation of the Urbach energy as a function of the composition (x) has different trends in the low- and high-ZnO glasses. It increases in the low-ZnO region, and decreases in the high-ZnO region (Fig. 9). As well known the Urbach energy reflects the degree of structural order or disorder (ordness or desordness) in amorphous materials [41]. The increase in Urbach energy in the low-ZnO region may be due to the increase in the depolymerisation of the glasses owing to the modifier effect of ZnO oxide. Conversely, in the high-ZnO region the value of ΔE decreases with the incorporation of ZnO in the glassy matrix suggesting that the disorder degree decreases in these glasses. As a matter of fact, vibrational spectroscopy and ionocovalency studies have shown that ZnO oxide in this composition region behaves as a former oxide and increases the crosslink density of the glasses. The occupation of former sites by zinc ions enhances the rearrangement of the different structural units and the formation of less disordered vitreous materials.

It is worth to note that the composition dependencies of the glass transition temperature and the gap energy show a minimum for the glass composition x = 20 mol%. Such a minimum mimics that observed in mixed alkali and mixed alkali–alkaline earth glasses [32, 34, 42]. Since the alkali ratio is maintained constant in the glasses under study ($Na^+/K^+ = 0.5$), one can ascribe the evolved minimum to the substitution of alkali ions (Na^+, K^+) by bivalent cations (Zn^{2+}) ions.

5 Conclusion

In this paper, we studied the system of glasses inside $(1-x)(NaPO_3–KPO_3)–xZnO$, $(0 \le x \le 50\%$ mol), these glasses were prepared by melt-quenching route. The density increases, however the molar volume decreases with increasing ZnO content. The glass transition temperature increases with the increase of the concentration of ZnO introduced in the glassy matrix, what is explained by the presence of P–O–Zn bonds which reticule the glassy structure. For x less than 20%, the glass transition temperature decreases owing to the small zinc–oxygen bonding energy. For larger x ($20 \le x \le 50$), the T_g increases because the covalent character of zinc–oxygen bonds. Raman and FTIR spectra show that the structure of the glasses contains different phosphate structural units and their contents depend on the composition. We can note also from these spectra that the addition of ZnO in the matrix ($NaPO_3–KPO_3$) leads to the depolymerisation, in other words, the conversion of metaphosphate units to pyrophosphate units. This conversion is assisted by the structural rearrangements in the vitreous network via the replacement of P–O–P and P=O bands by P–O–Zn bands. The variation of the optical band gap and Urbach energy depend on the glass composition. A minimum in E_g and a maximum in ΔE are observed for the glass composition (x = 20). The non-linearity of the glass transition temperature and these optical parameters with the composition are ascribed to the substitution of the alkali ions (Na^+, K^+) by the bivalent cations (Zn^{2+}) ions.

Acknowledgements The authors would like to thank the CNRST (Morocco) and OCP foundation for their financial support of this work in the framework of PPR project.

References

1. B. Tischendorf, J.U. Otaigbe, J.W. Wiench, M. Pruski, B.C. Sales, A study of short and intermediate range order in zinc phosphate glasses. J. Non Cryst. Solids **282**(2–3), 147–158 (2001)
2. R.V.S.S.N. Ravikumar, K. Ikeda, A.V. Chandrasekhar, Y.P. Reddy, P.S. Rao, J. Yamauchi, Site symmetry of Mn(II) and Co(II) in zinc phosphate glass. J. Phys. Chem. Solids **64**(12), 2433–2436 (2003)
3. G. Walter, U. Hoppe, J. Vogel, G. Carl, P. Hartmann, The structure of zinc polyphosphate glass studied by diffraction methods and31P NMR. J. Non Cryst. Solids **356**(43), 252–262 (2010)
4. P. Pascuta, G. Borodi, N. Jumate, I. Vida-Simiti, D. Viorel, E. Culea, The structural role of manganese ions in some zinc phosphate glasses and glass ceramics. J. Alloys Compd. **504**(2), 479–483 (2010)
5. E. Mansour, G. El-Damrawi, Electrical properties and FTIR spectra of ZnO-PbO-P2O5 glasses. Phys. B Condens. Matter. **405**(8), 2137–2143 (2010)
6. J.J. Hudgens, R.K. Brow, D.R. Tallant, S.W. Martin, Raman spectroscopy study of the structure of lithium and sodium ultraphosphate glasses. J. Non Cryst. Solids **223**(1–2), 21–31 (1998)
7. P.Y. Shih, S.W. Yung, T.S. Chin, Thermal and corrosion behavior of P_2O_5-Na_2O-CuO glasses. J. Non Cryst. Solids **224**(2), 143–152 (1998)
8. R. Morena, Phosphate glasses as alternatives to Pb-based sealing frits. J. Non-Cryst. Solids **264**, 382–387 (2000)
9. G. Tricot, B. Revel, S. Wegner, Thermal stability of a low Tg phosphate glass investigated by DSC, XRD and solid state NMR. J. Non Cryst. Solids **357**(14), 2708–2712 (2011)
10. J. Cha, T. Kubo, H. Takebe, M. Kuwabara, Compositional dependence of properties of SnO-P_2O_5 glasses. J. Ceram. Soc. Japan **116**, 915–919 (2008)
11. R. Oueslati, S. Krimi, J. Jacques, I. Khattech, A. El, M. Jemal, Structural and thermochemical study of Na_2O–ZnO–P_2O_5 glasses. J. Non-Cryst. Solids **390**, 5–12 (2014)
12. G.P. Singh, S. Kaur, P. Kaur, D.P. Singh, Modification in structural and optical properties of ZnO, CeO_2 doped $Al_2O_3PbOB_2O_3$ glasses. Phys. B Condens. Matter **407**(8), 1250–1255 (2012)
13. M.H.M. Zaid et al., Investigation on structural and optical properties of SLS–ZnO glasses prepared using a conventional melt quenching technique. J. Mater. Sci.: Mater. Electron. **26**(6), 3722–3729 (2015)
14. W.H. Zachariasen, Atomic arrangement in glass. Jour. Amer. Chem. Soc. **54**(10) 3841–3851 (1932)
15. M.S. Reddy, G.M. Krishna, N. Veeraiah, Spectroscopic and magnetic studies of manganese ions in ZnO-Sb_2O_3-B_2O_3 glass system. J. Phys. Chem. Solids **67**(4), 789–795 (2006)
16. W. Matz, D. Stachel, The structure of alkaline earth metaphosphate glasses investigated by neutron diffraction. J. Non-Cryst. Solids **101**, 80–89 (1988)

17. U. Cadi, A. Marrakech, En cotutelle et Spécialité: Physico-chimie de la Matière Condensée (2003)
18. R.K. Brow, D.R. Tallant, S.T. Myers, C.C. Phifer, The short-range structure of zinc polyphosphate glass. J. Non Cryst. Solids **191**(1–2), 45–55 (1995)
19. L. Montagne, G. Palavit, R. Delaval, Effect of ZnO on the properties of (100–x)($NaPO_3$)-xZnO glasses. J. Non Cryst. Solids **223**, 43–47 (1998)
20. Y. Zhang, Ionocovalency and applications 3. Ionocovalent cross-link density, pp. 1–6 (2011)
21. Y. Zhang, Ionocovalency and applications 1. Ionocovalency model and orbital hybrid scales, pp. 4381–4406 (2010)
22. M. El Hezzat, M. Et-tabirou, L. Montagne, E. Bekaert, G. Palavit, Structure and ac conductivity of sodium–lead–cadmium metaphosphate glasses. Mater. Lett. **58**, 60–66 (2003)
23. I. Konidakis, C.P.E. Varsamis, E.I. Kamitsos, D. Möncke, D. Ehrt, Structure and properties of mixed strontium-manganese metaphosphate glasses. J. Phys. Chem. C **114**(19), 9125–9138 (2010)
24. S.S. Das, V. Srivastava, Study of sodium and silver phosphate glasses doped with some metal chlorides. Prog. Cryst. Growth Charact. Mater. **52**(1–2), 125–131 (2006)
25. A.S. Budi, A.H. Permana, H. Nasbey, Y. Fujii, The characterization ZnO-Na_2O-P_2O_5 glass system for dental restorative materials. J. Tech. Soc. Sci. **1**(3), 47–55 (2017)
26. B.Ã. Eraiah, S.G. Bhat, Optical properties of samarium doped zinc–phosphate glasses. J. Phys. Chem. Solids **68**, 581–585 (2007)
27. M.A. Ghauri, S.A. Siddiqi, W.A. Shah, M.G.B. Ashiq, M. Iqbal, Optical properties of zinc molybdenum phosphate glasses. J. Non Cryst. Solids **355**(50–51), 2466–2471 (2009)
28. H. Es-sou, L. Bih, B. Manoun, P. Lazor, Structure, thermal analysis and optical properties of lithium tungsten-titanophosphate glasses. J. Non-Cryst. Solids **463**, 12–18 (2017)
29. E.A. Davis, N.F. Mott, Conduction in non-crystalline systems V. Conductivity, optical absorption and photoconductivity in amorphous semiconductors. Phil. Mag. **22**(179), 903–922 (1970)
30. F. Urbach, The long-wavelength edge of photographic sensitivity and of the electronic absorption of solids. Phys. Rev. **92**, 61 (1953)
31. N.H. Ray, Composition-property relationships in inorganic oxide glasses. J. Non-Cryst. Solids **15**(3), 423–434 (1974)
32. H. Bih et al., Thermal and structural studies of Li_2O-Na_2O-SrO-TiO_2-B_2O_3-P_2O_5 glasses by DTA, IR and EPR spectroscopy. J. Appl. Surf. Interfaces **1**, 57–63 (2017)
33. C. A. Gutierrez, Study of a mixed alkaline–earth effect on some properties of the CaO-MgO-Al_2O_3-SiO_2 system, no. May 2014 (2007)
34. F. Behrends, H. Eckert, Mixed-alkali effects in aluminophosphate glasses: a re-examination. J. Phys. Chem. C **3**, 17175–17183 (2011)
35. A.L. Allred, Electronegativity values from thermochemical data. J. Inorg. Nuclear Chem. **17**(1949), 215–221 (1961)
36. L. Bih, N. Allali, A. Yacoubi, A. Nadiri, A. Levasseur, Thermal, physical and spectroscopic investigations of P_2O_5—A_2MoO_4–A_2O (A = Li, Na) glasses. Phys. Chem. Glasses **40**(4), 229–234 (1999)
37. R.D. Shannon, Revised effective ionic radii and systematic studies of interatomic distances in halides and chalcogenides. Acta Cryst. **A32**, 751–767 (1976)
38. A. Chahine, M. Et-Tabirou, M. Elbenaissi, M. Haddad, J.L. Pascal, Effect of CuO on the structure and properties of (50–x/2) Na_2O-xCuO-(50–x/2)P_2O_5 glasses. Mater. Chem. Phys. **84**(2–3), 341–347 (2004)
39. J.O. Byun, B.H. Kim, K.S. Hong, H.J. Jung, S.W. Lee, A.A. Izyneev, Properties and structure of RO-Na_2O-Al_2O_3-P_2O_5(R = Mg, Ca, Sr, Ba) glasses. J. Non Cryst. Solids **190**(3), 288–295 (1995)
40. B. Bae, M.C. Weinberg, Ultraviolet optical absorptions of semiconducting copper phosphate glasses. Ultraviolet glasses optical absorptions of semiconducting copper phosphate. J. Appl. Phys. **7760**(1993), 0–7 (2014)
41. S.F. Khor, Z.A. Talib, W.M.M. Yunus, Optical properties of ternary zinc magnesium phosphate glasses. Ceram. Int. **38**(2), 935–940 (2012)
42. G. Srinivas, J.S. Kumar, M.N. Chary, R. Sayanna, EPR and optical studies on binary mixed alkali alkaline earth oxide borate glasses doped with Cu^{2+} ions. Glass Phys. Chem. **42**(2), 141–148 (2016)